NASA TECHNICAL MEMORANDUM

NASA TM X-52219

NASA TM X-52219

FEASIBILITY STUDIES OF SPACE RADIATORS USING VAPOR CHAMBER FINS

by Henry C. Haller and Seymour Lieblein
Lewis Research Center
Cleveland, Ohio

TECHNICAL PAPER proposed for presentation at
Heat Pipe Conference sponsored by the Atomic
Energy Commission and Sandia Laboratories
Albuquerque, New Mexico, June 1, 1966

NATIONAL AERONAUTICS AND SPACE ADMINISTRATION · WASHINGTON, D.C. · 1966

FEASIBILITY STUDIES OF SPACE RADIATORS USING VAPOR CHAMBER FINS

by Henry C. Haller and Seymour Lieblein

Lewis Research Center
Cleveland, Ohio

TECHNICAL PAPER proposed for presentation at

Heat Pipe conference sponsored by the Atomic Energy Commission and Sandia Laboratories
Albuquerque, New Mexico, June 1, 1966

NATIONAL AERONAUTICS AND SPACE ADMINISTRATION

FEASIBILITY STUDIES OF SPACE RADIATORS

USING VAPOR CHAMBER FINS

By Henry C. Haller and Seymour Lieblein

Lewis Research Center
National Aeronautics and Space Administration
Cleveland, Ohio

E-3542

INTRODUCTION

A major problem in the design of large electric space powerplants using a closed power cycle such as the Rankine turbogenerator concept is the efficient and reliable rejection of large amounts of waste heat by radiation to space. Since the rejection of waste heat is radiation-limited, the resulting radiator surface areas and weights are generally large. The large radiator areas in conjunction with the meteoroid hazard in space also imply the need for some degree of protection for the vulnerable (fluid-carrying) surfaces, which results in further increases in radiator weight.

Radiators designed for the rejection of waste heat generally employ thin solid fins as an extended radiation heat-transfer surface between fluid-carrying tubes as illustrated by the direct-condensing radiator in figure 1 (refs. 1 to 5). In this configuration, vapor from the cycle turbine exhaust is distributed to the finned tubes by a vapor header. The heat radiated from the finned tubes and the vapor header causes the vapor to condense. The condensate is then subcooled and collected in the liquid header for return to the cycle via the condensate pump.

The purpose of such a fin-tube arrangement is to reduce the amount of the overall radiator surface occupied by flow passages and thereby reduce the area vulnerable to critical damage from impacting meteoroids. In such configurations, the fins receive heat from the fluid-carrying tubes by conduction, and heat is lost by radiation to space resulting in temperature drops along the length of the fin between adjacent tubes. As a consequence, the overall radiating effectiveness of the radiator is reduced, and the required radiator planform area and weight are increased. In addition, the thermal gradients in the fin give rise to undesirable thermal stresses. Typical solid conducting fin radiators are the central, open, and double fin-tube configurations shown in figure 2.

The vapor-chamber fin concept proposes to reduce radiator area and weight by providing for an essentially isothermal fin between tubes (refs. 6, 7, and 8). It accomplishes this by replacing the solid fin with a double-wall fin that forms a hollow chamber which can then operate as a heat pipe between the tube (boiling) surface and the fin (condensing) surface.

The objective of this paper is to present some results of feasibility studies of space radiators incorporating vapor chamber fins, as intended for application to Rankine system powerplants. Included in the presentation are: (1) a comparison of the weight and geometry characteristics of several vapor-chamber-fin and conducting-fin radiators; (2) an indication of the sensitivity of vapor-chamber radiator weight to capillary flow variables; (3) a compilation of capillary internal-flow requirements; and (4) a discussion of anticipated problem areas.

SYMBOLS

A_p radiator planform area, sq. ft.

D_o tube outer diameter, ft.

g gravitational constant, 32.2 lb_m ft/lb_f sec^2

H heat of condensation or vaporization, BTU/lb

h heat transfer coefficient, BTU/hr-sq. ft.-^oF

J mechanical equivalent of heat, 778 ft-lb/BTU

k thermal conductivity, BTU/ft-hr-^oF

K_H fluid turning loss factor for flow from header to tubes

l half fin length, ft

Pe electrical power output, KW

$P(0)$ non-penetration probability

Q heat rejection rate, BTU/hr

R_b tube sidewall to tube centerline dimension, $R_o - \left[1 - (\delta_s/\delta_a)\right] \delta_a$, ft

R_o tube outer wall to tube centerline dimension, ft

S fin to tube separation distance, ft

T temperature, ^oR

T^* static fluid temperature at tube inlet, ^oR

t fin thickness, ft

u_o velocity of vapor at tube inlet, ft/sec

W weight, lbs

Z	tube length, ft
δ	thickness, ft
ϵ	surface emittance
σ	Stefan-Boltzman constant, 1.713×10^{-9} $\frac{\text{BTU}}{\text{sq.ft. hr } {}^{\circ}R^4}$

Subscripts

a	tube armor
B	boiling
b	tube block surface
C	condensing
f	fin
o	outside surface
R	radiator inlet
S	saturation
s	tube side wall
t	tube

ANALYSIS

Configurations

The general radiator configuration considered for the analysis is a flat direct-condensing radiator applicable to Rankine power cycles similar to the configuration shown in figure 1. Solid conducting fin-tube geometries of interest were shown in figure 2, and two forms of vapor chamber fins are shown in figure 3. In both cases of figure 3, the principle of operation is the same. The two rectangular fins form a sealed enclosed chamber between adjacent tubes. A capillary-flow medium such as narrow grooves, woven wire mesh, or fibrous mat, lines the inner surfaces of the fin chamber and is saturated with a heat-transport fluid. The working fluid in the chamber is boiled off the tube surfaces at temperature T_b, condensed on the fin surfaces at temperature T_f, with the condensate return provided by the capillary pumping which presumably is essentially insensitive to gravity forces. In addition, the fluid used should provide a saturation pressure corresponding to the chamber operating temperature that is structurally compatible with the chamber construction.

The block vapor fin geometry shown in figure 3(a) is constructed of a corrosion-resistant inner liner tube surrounded by a block of armor material to which the fins are attached. For this block vapor fin geometry, the liner can be damaged by impacting meteoroids in two general ways. The first of these is by any primary impacts occurring on the outer exposed surfaces of the tube block. These impacts are assumed to obey the conventional armor penetration and damage relations developed for completely exposed tubes. The required armor thickness, δ_a , is applied in full on the upper and lower surface of the tube.

A second damage source can arise from a spray of particles on the armor block side surface area resulting from impacts on the fin surfaces. In view of the bumper action involved and the obliquity of the secondary impacts, however, a reduction will undoubtedly be allowed in the armor thickness required by the tube block side wall, δ_s , to resist the effects of these secondary impacts. A significant parameter δ_s/δ_a is therefore defined as the ratio of the minimum armor thickness retained on the enclosed side of the tube block to the armor thickness on the exposed side.

The bumper vapor fin-tube configuration of the lower part of figure 3 proposes to use the fins as a bumper against impacting meteoroids over the complete tube periphery. It accomplishes this by using the fins as continuous sheets separated from the tubes by a thin strut. In this manner, no portion of the tube outer surface is directly exposed to impact. Accordingly, relatively thin tube walls may be allowed with a subsequent reduction in radiator weight, and a completely monometallic construction can be used for ease of fabrication. For this configuration, the parameter δ_s/δ_a refers to the ratio of tube wall thickness to the thickness of armor that would be required if the upper tube surface had been directly exposed, as in the case of the block configuration.

Recent preliminary results of hypervelocity impact tests of the bumper principle of meteoroid protection (3/32-inch diameter pyrex projectiles at 25,000 feet per second) have shown substantial allowable reductions in tube side-wall thickness, with indicated design values of δ_s/δ_a well below 0.5. For stainless steel and stainless-steel clad copper bumper fins of around .018 inch thickness, inner-surface spalling in a stainless steel tube was suppressed with tube wall thicknesses of as small as 0.060 inch.

Inasmuch as the vapor chamber will lose its heat-transport action if a puncture and loss of transport fluid occur, the long fin chambers are divided longitudinally into a number of sealed segments by numerous transverse bulkheads to reduce the hazard as illustrated in figure 4. The thickness of the fin was based on the number of segments involved (a variable) and a selected probability that a certain percentage of the segments would remain unpunctured at the end of the design lifetime of the radiator. The actual dimensions of the fin result from the radiator weight optimization procedure.

Assumptions and Approach

The analysis of vapor chamber fin radiator characteristics is based on the principal assumption of a steady-state heat transport within the vapor chamber with uniform vapor saturation temperature. Further specific assumptions used in the development of the heat-transfer relations for the vapor-chamber fin-tube geometries are:

(1) The radiator outer surfaces act as grey bodies with emitted radiation governed by Lambert's cosine law.

(2) Hemispherical radiation to space is from both outer surfaces of the radiator to a $0^{\circ}R$ space sink temperature.

(3) The tube outer surface temperature and fin temperature are constant along the length of the tube.

(4) There is no temperature drop across the tube liner.

(5) The boiling and condensing heat-transfer coefficients on the chamber surfaces are known and will be varied parametrically.

(6) The transverse bulkheads are adiabatic surfaces.

(7) The temperature of the fin surfaces and each block surface is uniform.

(8) Material properties such as thermal conductivity, modulus of elasticity, and emittance are constant and based on the radiator vapor inlet temperature.

(9) The inside tube wall temperature is uniform circumferentially and equal to the static temperature of the fluid evaluated at the inlet conditions of the tube.

(10) Additional heat input to the fin by conduction from the tube block or strut and by radiation from the tube side-wall surface is negligible.

The overall heat transfer path is as follows: The cycle working fluid in the tube gives up its heat to the inner surface of the tube by condensation.

$$T^* = T_R\left(1 - \frac{1}{2}\frac{K_H u_O^2}{J g H}\right) \tag{1}$$

For the block vapor chamber fin, part of this heat travels by conduction to the outer surfaces of the tube block according to the simplified relation.

$$Q_b = \frac{2R_b k}{\delta_a}(T^* - T_b)Z \tag{2}$$

and is radiated to space according to

$$Q_b = 2\sigma \epsilon R_b T_b^4 Z \tag{3}$$

The remainder of the heat from the condensing fluid is conducted to the tube block side wall

$$Q_s = \frac{2k\,(R_o - t)}{\delta_s}\,(T^* - T_b)Z \tag{4}$$

where it is then transferred to the fin surfaces by the boiling of the capillary heat-transport fluid on the block surface

$$Q_B = 2h_B\,(R_o - t)(T_b - T_S)Z \tag{5}$$

Condensing of the fluid on the fin surfaces takes place according to

$$Q_C = 2h_C\,l(T_S - T_f)Z \tag{6}$$

This heat is then radiated to space from both the upper and lower fin surfaces of length l

$$Q_f = 2\sigma \epsilon\, l\, T_f^4 Z \tag{7}$$

Thus, since $Q_f = Q_C = Q_B$, equations (5), (6), and (7) can be solved for the fin temperature T_f. The resulting expression is:

$$T_f + \frac{\sigma\epsilon}{h_B}\left(\frac{l}{R_o - t} + \frac{h_B}{h_C}\right) T_f^4 = T_b \tag{8}$$

The bumper vapor chamber fin action is essentially the same, with the exception that all heat released in the tube is transferred by boiling off the tube outer surfaces.

Radiator solutions using the results of the analysis were obtained from an iterative procedure programmed into an electronic digital computer. The approach and procedure used were the same as that in references 2 and 6. The optimization procedure which yielded minimum radiator weight involved heat transfer relations, meteoroid protection, cycle condensing fluid pressure drop, and header, tube, and fin weights. Specific program inputs required for the two vapor chamber fin radiators were: tube internal diameter; vapor temperature at radiator inlet, T_R; cycle power level and conditions; properties of materials of construction and cycle fluid; meteoroid protection constants; vapor-chamber boiling and condensing heat-transfer coefficients; vapor-chamber segment planform area; capillary material weight; tube wall thickness ratio δ_s/δ_a; pressure drop in the tubes and headers; and the chamber bulkhead thickness. Additional program inputs required for the bumper vapor chamber fin are the separation distance between the fins and

the tubes, and the strut thickness between the tube and fin. The latest meteoroid hazard information and hypervelocity impact relations generated at the NASA Lewis Research Center (refs. 9 and 10) were used as inputs for the results presented in the paper.

RESULTS AND DISCUSSION

Block and bumper vapor chamber fin-tube geometries along with central and double fin solid-conducting configurations constructed of several materials have been analyzed for application to a direct-condensing Rankine cycle radiator. Principal consideration was given to a 500-KW output cycle with potassium working fluid and a radiator temperature of 1700°R. Calculations were also made for a 30-KW steam cycle with an aluminum radiator at 870°R in order to obtain an indication of relative radiator performance at low temperatures with the use of the same computer program.

A 500 day mission time and tube nonpenetration probabilities $P(0)_t$ of 0.90 to 0.995 were chosen for the calculation of the tube armor thickness. For the block vapor chamber fin radiator, a probability of 0.90 was specified that 75 percent of the segmented vapor fin chambers would remain unpunctured by the end of the mission time. The bumper vapor chamber fin radiator had a probability of 0.95 that 90 percent of the chambers would be unpunctured at the end of the mission. A tube block side wall to maximum armor thickness ratio $\delta_s/\delta_a = 0.5$ was chosen for the calculations along with a value of fin to tube separation ratio for the bumper fin geometry S/D_o of 0.5. The armor thickness for the tubes was calculated for the incipient spall condition. This value of armor thickness was considered adequate to prevent perforation, but not sufficient to guarantee that there will not be spalling off the tube inner surface. For the segmented vapor chamber fins, the fin wall thickness corresponded to a value just equal to the thickness that will be penetrated by the meteoroids.

Pressure drop ratios were set at $\Delta P/P = 0.02$ for the vapor header and $\Delta P/P = 0.05$ for the radiator tubes. The emittance of the radiator surface was taken to be 0.90.

Results presented include comparisons of radiator weight and geometry, sensitivity of vapor chamber radiator design to capillary variables, and capillary heat flux and flow rate requirements.

Radiator Weight

A comparison of minimum radiator specific weights for the solid-conducting central fin, and the block and bumper vapor chamber fin-tube configurations for a 500-KW cycle with a 1700°R stainless-steel radiator is shown in figure 5 for a variation in tube nonpenetration probability from 0.90 to 0.995. The vapor chamber fin radiators are seen to yield substantially lower specific weights than the solid conducting central fin geometry. The large difference in specific weight between the solid

conducting central fin and the vapor chamber fin radiators is caused by the poor thermal conductivity of stainless steel fin and the greater extent of armor required (full tube periphery coverage) in the case of the central fin tube geometry. The bumper vapor fin radiator produced a lighter weight than the block vapor fin, since the reduction in the extent of armor coverage more than offset the added weight of the strut between the fin and the tube.

The comparison of figure 5 is actually a conservative one, since recent hypervelocity impact data indicates that values of δ_s/δ_a as low as 0.25 may be allowable for bumper fin design. For $\delta_s/\delta_a = 0.25$, the bumper fin radiator specific weight would be reduced by around 15 percent. Thus, specific radiator weights of 2 lbs/KW are achievable with this configuration. Futhermore, at these lower values of δ_s/δ_a , the tube wall thicknesses required for meteoroid protection is about the same as that required for structural reasons.

The curves for the two vapor chamber fin geometries of figure 5 were calculated for the case of the same initial power, that is, neglecting the effect of fin punctures on radiator heat rejection capability. When a vapor chamber fin segment is punctured, it will lose its capillary fluid and hence will no longer operate as a vapor chamber fin. However, the fins of the chamber will receive heat by conduction from adjacent tubes and fins and by radiation from the adjacent tube and bulkhead surfaces. Thus, a radiation capability comparable to a solid conducting fin will be maintained. Solution of the actual physical case of a punctured segment requires a detailed two-dimensional study of the fin chamber heat transfer. However, for simplicity, calculations of degraded radiation for the vapor chamber radiators were restricted to one-dimensional heat transfer along the fins for the case of isolated chamber puncture (adjacent segments operative). Analyses for the more complex case of adjacent segment punctures are given in references 6, 7, and 8.

Figure 6 shows the calculated variation of ratio of final to initial heat rejection of the radiator as a function of percent of surviving segments at the end of the mission. The results indicate, as expected, that the ratio of final to initial heat rejection also depends on the thermal conductivity of the fin material. For the same material, as shown by the two lower curves, the bumper vapor fin yields a greater reduction in final heat rejection because of the added thermal resistance of the struts separating the fin and tube (fig. 3). The decrease in the heat rejection ratio with decreasing surviving segments is brought about by a decrease in fin wall thickness accompanying the decrease in survival percentage as well as by the decrease in non-punctured area.

In some instances it may be desirable to maintain a constant heat rejection load throughout the lifetime of the powerplant. Thus, vapor chamber fin radiators must be designed for fixed final heat rejection. If constant radiator temperature is also specified this would require an overdesign of the vapor chamber fin radiators, that is, an increase in area above that

required for the no-puncture case presented in figure 5. Thus, an increase in radiator specific weight will be incurred compared to the solid-conducting fin radiators which undergo no comparable thermal degradation.

An indication of the increase in vapor chamber radiator weight when designed for constant final heat rejection capability can be obtained, if it is assumed for simplicity that the percentage increase in required area (and therefore weight) is equal to the percentage decrease in final heat rejection as given in figure 6. A comparison of radiator specific weight for the two cases of fixed initial and final heat rejection is shown in figure 7 for stainless steel radiators. The difference in required weight between the central fin and bumper vapor chamber fin radiators is still quite large for this example.

When high thermal conductivity fin materials such as stainless steel-clad copper can be used for the solid conducting fin geometries, the weight reduction indicated by the use of a block vapor chamber fin is diminished, as shown in figure 8. The decrease in specific weight of the central fin radiator in this figure compared to that of figure 5 is attributed to the higher thermal conductivity of the clad copper. The larger weight for the clad vapor fin compared to the stainless steel case in figure 5 is due to the greater fin thickness required by the clad copper to resist perforation at the radiator operating temperature (low strength of copper). Specific weight variations for the bumper vapor chamber fin radiator with clad copper fins have not yet been made. However, the bumper configuration weight is expected to be less than for the block configuration as in the case of figure 5.

The comparative weight situation for a low temperature Rankine cycle is illustrated in figure 9. For this case, the block vapor chamber fin radiator indicates a substantial weight reduction only for relatively high values of tube non-penetration probability. For low power and temperature designs, the tube meteoroid armor protection constitutes a smaller percentage of the total radiator weight than for high power designs. Thus reductions in total radiator weight due to the reduced armor requirements of the vapor fin configuration are not as pronounced as for high power cases. Furthermore, the use of high termal conductivity aluminum permits a reduced minimum weight design in the case of the solid-conducting central fin radiator. Thus, large differences in radiator weights appear only when $P(0)_t$ and the armor requirements are relatively high.

Planform Area

The comparison of planform area between conducting fin and vapor chamber fin designs can best be made on the basis of plots of specific planform area (ft^2/KW) and specific weight against tube inside diameter. Representative plots for two 500-KW cycle cases and a 30-KW case are shown in figures 10, 11, and 12, respectively. Also shown on the figure are the number of tubes corresponding to the minimum-weight and end point diameters. For the high

power level cases, the principal general observation is that very little difference in planform area is indicated between the central fin and vapor chamber fin geometries at minimum radiator specific weight. However, if a large tube diameter is considered in order to reduce the number of radiator tubes involved, the vapor chamber fin geometries can produce a sizable reduction in planform area (10 to 15 percent) with least penalty in increase in specific weight.

For the low-power-level, low-temperature level-case (fig.12), the block vapor fin offers a sizable reduction in planform area (23 to 35 percent) over the entire range of tube inside diameters investigated. In all three cases, the effect of tube non-penetration probability on the planform area comparisons of the vapor fin and central fin geometries was small.

Sensitivity to Capillary Variables

Vapor chamber capillary variables such as boiling and condensing heat transfer coefficients, capillary material weight, number of fin segments, and segment bulkhead thickness directly affect radiator planform area, and specific weight. The effect of the boiling heat transfer coefficient at the tube surface of the fin chamber on the fin temperature is shown in figure 13. Curves are given for high and low temperature level radiators for three values of the ratio of chamber condensing to boiling heat transfer coefficients. All cases considered show a rapidly decreasing fin temperature with decreasing boiling heat transfer coefficient. The high-temperature level radiator exhibits a larger drop in fin temperature than the low-temperature radiator at a low condensing coefficient (low value of $\frac{h_C}{h_B}$). (The results presented in the previous curves were based on boiling and condensing heat transfer coefficients of 10^4 BTU/hr-ft^2-$^\circ$R.)

The effect of the boiling heat transfer coefficient on radiator planform area is shown plotted in figure 14 for the bumper and block vapor chamber fin geometries. The radiator area, expressed as the ratio of the planform area to the planform area for infinite heat transfer coefficients is seen to increase markedly with decreasing boiling heat transfer coefficient for both configurations. This in essence is a reflection of the fourth power variation of the fin to tube temperature ratio shown on figure 13. The block vapor fin has a smaller planform area ratio than the bumper configuration because the tube block area has a higher outer surface temperature (no strut). The corresponding variation of relative radiator weight with boiling heat transfer coefficient is illustrated in figure 15 for both vapor chamber fin-tube geometries. As expected the weight curves closely follow the area variations.

Another variable of interest is the internal chamber capillary weight which is assumed to be composed of the weight of the capillary material plus the contained heat transfer fluid. Figure 16 shows a plot of vapor fin

capillary weight versus the ratio of radiator weight to radiator weight with zero capillary weight. It is seen that capillary weight can exert a large influence on the total radiator weight. For the calculations shown in the previous figures, the capillary weight was selected as 0.2 lbs/sq ft.

The effect of the number of vapor fin segments and the fin chamber bulkhead thickness on radiator specific weight at the minimum weight condition was found to be relatively small for the range of conditions investigated. The high temperature level block and bumper vapor fin cases required around 1000 fin segments for a reasonable fin chamber configuration. Only a 4 to 6 percent variation in radiator specific weight occurred if the number of fin segments varied from 500 to 2500. The smaller number of segments resulted in an increased weight, since fin chamber wall thickness increased as required by meteoroid penetration considerations. Typical calculated values of fin thickness were around 0.015 to 0.025 inches in this range of number of segments. For 1000 fin segments the fin thickness is around 0.018 inch.

Increasing the bulkhead thickness from 0.020 to 0.060 inches resulted in about a 13 percent increase in weight for the bumper vapor chamber fin geometry. For the block vapor fin radiator the percent increase in weight will be less. The specific value of bulkhead thickness required for a design will depend on structural considerations.

Capillary Requirements

The capillary performance requirements for the vapor chamber are determined by the heat flux at the boiling surface and the latent heat of vaporization of the capillary fluid chosen. The boiling heat flux is determined by means of the previously indicated heat balance within the fin chamber (eqs. (4), (5), (6) and (7)). Sample results for high and low temperature and power level systems at the minimum weight condition are given in table I. (Boiling heat fluxes varied only slightly with some of the radiator design variables.) It is observed from the table that for all block and bumper vapor fin cases considered, the boiling heat flux ranged from 3 to 7×10^4 BTU per hour per square foot. Information available in the literature indicates such values of heat flux may be attainable. A test of capillary wick with sodium at approximately 2000° R had produced a limiting heat flux of 9.5×10^4 BTU per hour per square foot after which local over-heating occurred (ref. 13). Other tests using water as the capillary fluid (ref. 14) have yielded a heat flux of around 1×10^5 BTU per hour per square foot.

Once the boiling heat flux has been calculated, the required capillary fluid mass flow rate for the vapor chamber can be obtained knowing that mass flow rate is directly proportional to heat flux and inversely proportional to the latent heat of vaporization of the fluid. Table I gives flow rates for several liquid metals and other applicable fluids expressed in units of pounds per hour per foot of tube length. The capillary material system selected will have to be capable of continuously supplying these indicated flow rates in order to achieve steady-state operation.

Another important consideration of the vapor fin chamber is the length of the capillary flow path. Typical values for the 500-KW high-temperature radiator systems are flow lengths of 4 to 5 inches at the minimum weight condition. The 30-KW low-temperature radiator system required flow lengths of 25 to 30 inches for the minimum weight geometry.

Possible Problem Areas

The preceding results have indicated some attractive advantages for the vapor chamber fin radiator. However, it is recognized that several unknown factors and possible problem areas may exist in the successful development of such configurations. Principal concern is with internal capillary flow, and materials and structure.

The principal question posed by the analysis is the selection of suitable capillary materials and fluids that will satisfy steady-state wicking permeability, boiling heat flux, weight, and flow-length requirements in a zero-gravity environment. The attainment of high boiling and condensing heat transfer coefficients ($> 10^4$ BTU/hr-ft^2-^{o}F) was strongly indicated, which for the boiling surfaces, requires the avoidance of film boiling or burnout. Attention must also be given to the start-up process, especially if a liquid metal heat transport fluid is used, because of the frozen state of these fluids at ambient temperatures. Experimental and theoretical investigation is therefore indicated in order to establish the feasibility of the capillary internal flow for these radiator applications.

The simplified internal heat transport relations used in the preceding analysis were based on the assumption of uniform temperature and heat fluxes over the boiling and condensing surfaces, which implies negligible flow and temperature gradients within the vapor chamber. Such an approximation may be suitable for a direct-condensing radiator in which the working fluid temperature remains essentially constant along the length of the tube. However, there are other situations where relatively large temperature variations and consequently large internal gradients may be imposed on the fin chamber boundaries. One such situation occurs for a vapor chamber segment when an adjacent segment is punctured, and the common surfaces become cooler than the other surfaces. The more significant variable-temperature situation would occur in the design of vapor chamber fins for single-phase flow radiators such as the liquid-flow radiators for indirect heat rejection cycles. It is not clear how best to design for the axial variation in temperature along the tube. If a short axial distance is used between chamber bulkheads to reduce axial temperature gradients, then an excessively large number of segments will be required. The use of separated and insulated segments can also be considered, but such an arrangement forfeits the conducting potential of the segment in the event of a puncture. An understanding of capillary chamber performance under non-uniform boundary temperature is therefore also desirable.

A second consideration and potential problem area is that of materials and structure. Proper selection must be made of capillary material, fin material, and heat transport fluid in order to avoid long-term corrosion and contamination effects on capillary performance. Also, for the geometric configurations considered, fabrication techniques must insure proper sealing of a large number of individual fin segments during both long-term steady-state operation and start-up transient conditions. Finally, the structural integrity of the box-like structure of the vapor chamber fin segment may require detailed attention. Preliminary analysis of the deflection of typical fin sections under an ambient pressure differential (as would occur during vacuum fill on the ground) indicated the possible need for additional structural support. Required values of segment bulkhead and strut thicknesses also have not been firmly established.

CONCLUDING REMARKS

The preceeding preliminary results of feasibility studies of an application of the vapor chamber fin or heat pipe-concept to Rankine-cycle space radiator design have indicated an attractive potential advantage over the solid conducting fin configurations. The indicated weight reductions were most pronounced for high power level systems ($\geq$ 500 KW) with very high design values of radiator non-penetration probability (>0.98). However, several unknowns and possible problem areas were recognized to exist with respect to capillary internal flow, materials, and structure. Further research will be required to establish the practicality of such designs.

It must be pointed out, however, that the studies reported herein were conducted for direct-condensing radiators, and it is not known whether the results obtained are also valid for single-phase flow radiators. Liquid-flow radiators may be different than condensing-vapor radiators in three significant respects. (1) Variations in temperature along the tube; (2) generally lower values of radiator panel non-penetration probability when segmenting is used; and (3) smaller tube diameters. These factors might tend to produce a different and possible poorer advantage for the vapor chamber radiator. Comparable feasibility studies of single phase radiators are therefore in order.

REFERENCES

1. Reynolds, W.C.: A Design-Oriented Optimization of Simple Tapered Radiating Fins. Journal of Heat Transfer (ASME Trans.), Ser. C., Vol. 85, No. 3, August 1963, pp. 193-202.

2. Krebs, Richard P.; Haller, Henry C.; and Auer, Bruce M.: Analysis and Design Procedures for a Flat, Direct-Condensing, Central Finned-Tube Radiator. NASA TN D-2474, 1964.

3. Dennington, R.J., et al: Space Radiator Study. ASD Technical Report 61-697, April, 1962.

4. Haller, Henry C.: Comparison of Heat-Rejection and Weight Characteristics of Several Radiator Fin-Tube Configurations. NASA TN D-2385, 1964.

5. Haller, Henry C.: Analysis of a Double Fin-Tube Flat Condenser-Radiator and Comparison with a Central Fin-Tube Radiator. NASA TN D-2558, 1964.

6. Haller, Henry C.; Lieblein, Seymour; and Lindow, Bruce G.: Analysis and Evaluation of a Vapor-Chamber Fin-Tube Radiator for High-Power Rankine Cycles. NASA TN D-2836, 1965.

7. Haller, Henry C.; Lindow, Bruce G.; and Auer, Bruce M.: Analysis of Low-Temperature Direct-Condensing Vapor-Chamber Fin and Conducting Fin Radiators. NASA TN D-3103, 1965.

8. Lindow, Bruce G.; and Lieblein, Seymour: Analysis of a Bumper-Fin Vapor Chamber Fin-Tube Radiator for High Power Rankine Cycles. NASA TN to be published.

9. Clough, Nestor; McMillan, A. R.; and Lieblein, Seymour: Material and Geometry Aspects of Meteroid Armor Protection for Space Radiator Tubes. NASA TM X-52186, 1966.

10. Lieblein, Seymour: Material and Geometry Aspects of Space Radiators. NASA TN to be published.

11. Haller, Henry C.; and Lindow, Bruce G.: Comparison of Vapor Chamber Fin Radiators Using Stainless Steel, Columbium, and Stainless Steel-Clad Copper Fins. NASA TN to be published.

12. Haller, Henry C.; and Lindow, Bruce G.: Comparison of Central, Double, and Vapor Chamber Fin-Tube Radiators Using Stainless Steel-Clad Copper Fins. NASA TN to be published.

13. Grover, G. M.; Cotter, T. P.; and Erickson, G. F.: Structures of Very High Thermal Conductance. Journal of Applied Physics, Vol. 35, No. 6, July 1965, pp. 1990-1991.

14. Langston, L. S.; Sherman, A.; and Hilton, B. H.: Second Quarterly Report - Vapor Chamber Fin Studies. NASA CR-54922, PWA-2773, January 1966.

TABLE I. - CAPILLARY REQUIREMENTS FOR MINIMUM WEIGHT DISIGNS

Radiator type	Power level, P_e, kW	Temperature, ^{o}R	Boiling heat flux, Btu/hr-sq ft	Heat transfer fluid	Flow rate, lb(hr)(ft)
Aluminum (Block)	30	860	4.4×10^4	Diphenyl Water	16.0 2.0
Stainless Steel (Block)	500	1700	6.6×10^4	Potassium Sodium Lithium	5.60 2.77 .53
S.S. Clad Copper (Block)	500	1700	6.5×10^4	Potassium Sodium Lithium	5.48 2.71 .51
Stainless Steel (Bumper)	500	1700	3.75×10^4	Potassium Sodium Lithium	5.5 2.5 .5

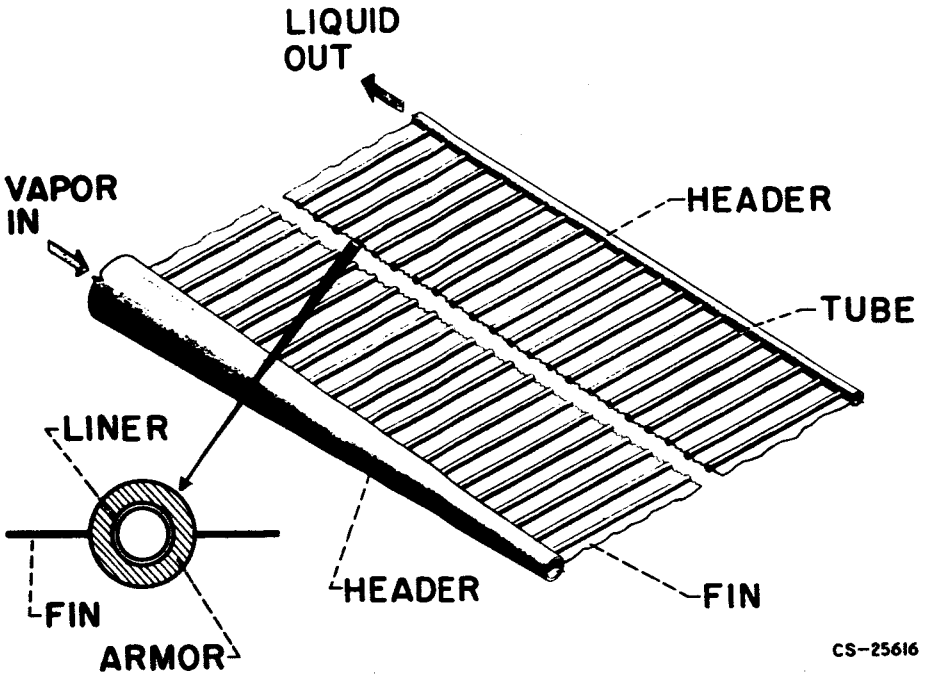

Figure 1. - Fin-and-tube radiator.

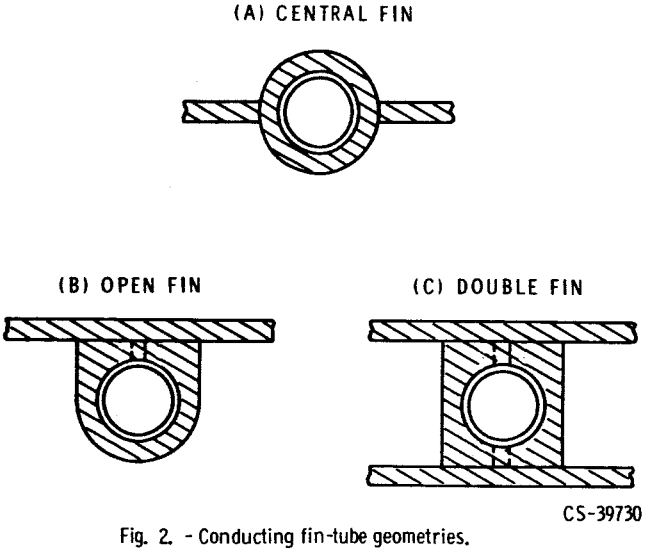

Fig. 2. - Conducting fin-tube geometries.

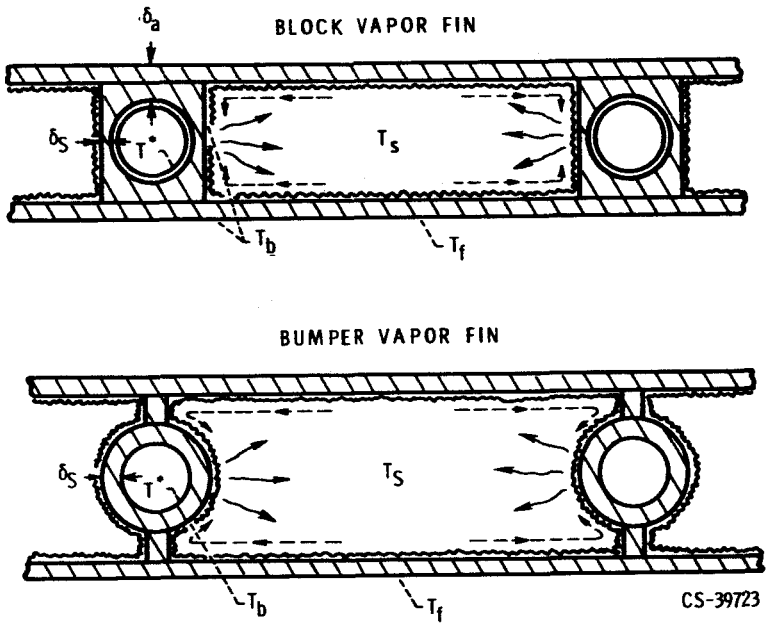

Fig. 3. - Vapor chamber fin-tube geometries.

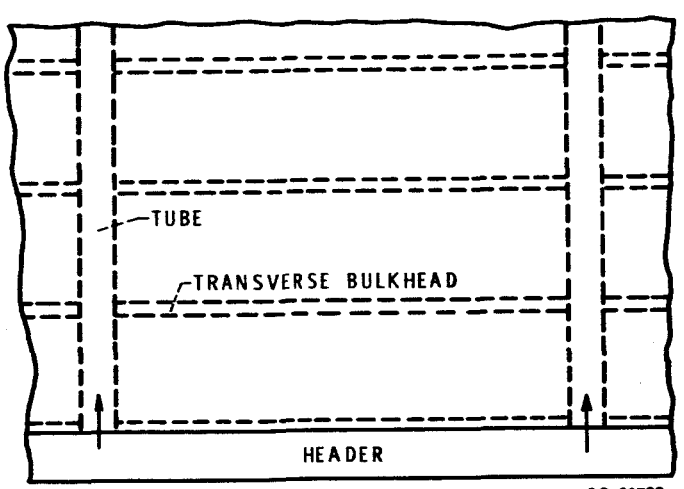

Fig. 4. - Vapor chamber fin segment arrangement.

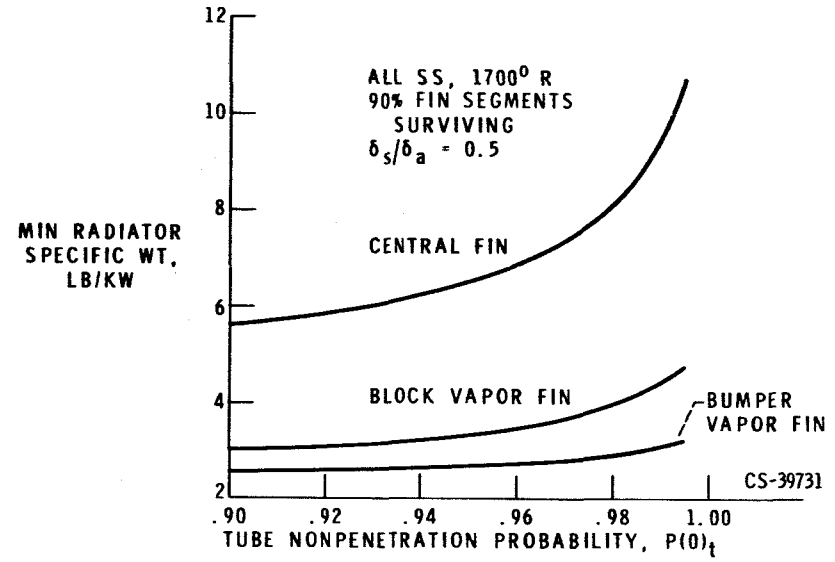

Fig. 5. - Radiator weight comparison for 500 kw Rankine cycle. Same initial power.

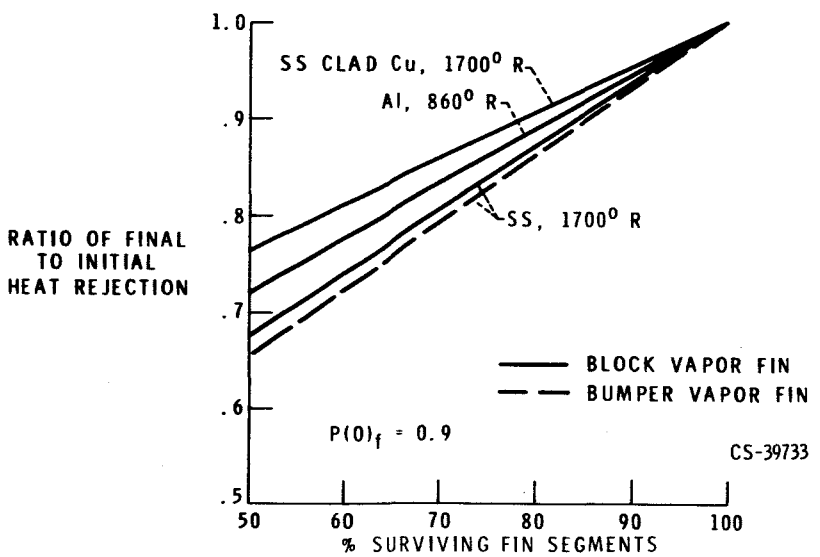

Fig. 6. - Effect of number of surviving segments on radiator final heat rejection.

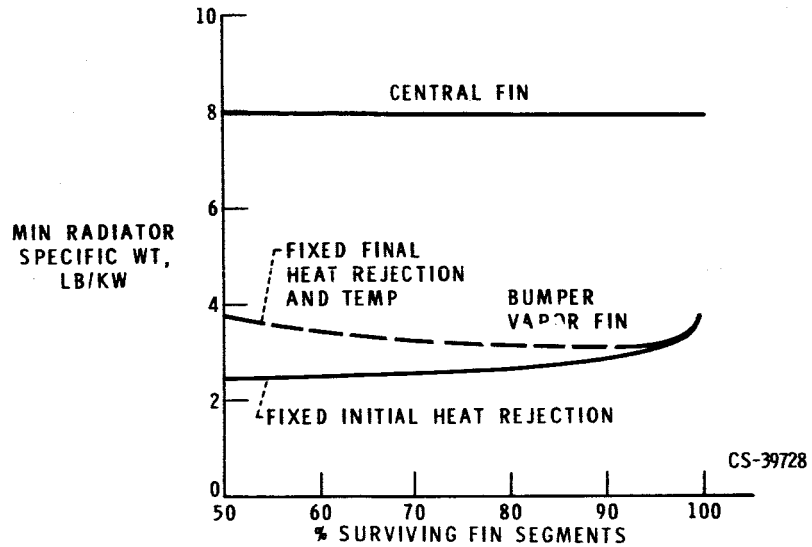

Fig. 7. - Effect of surviving segments on radiator weight, 500 kw Rankine cycle; ss radiator; $P(0)_f = 0.90$; $P(0)_t = 0.98$.

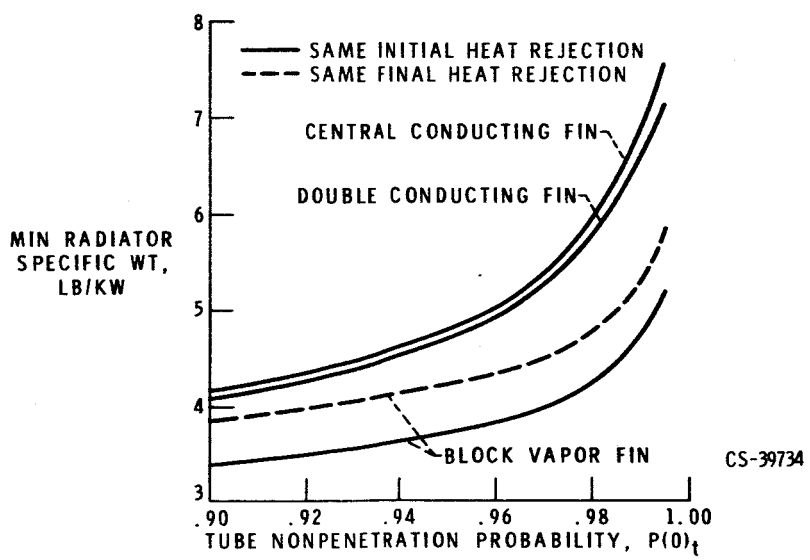

Fig. 8. - Radiator weight comparison, 500-kw Rankine cycle ss clad copper fins, 1700° R, 75% fin segments surviving.

E-3542

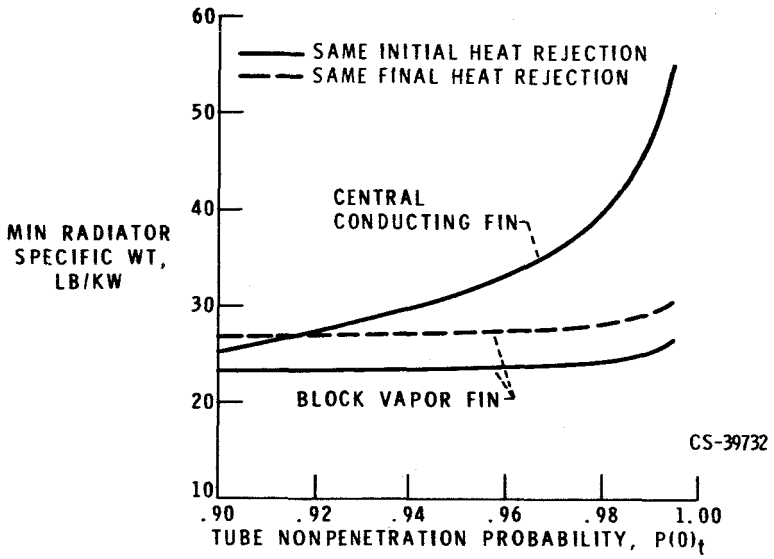

Fig. 9. - Radiator weight comparison, 30-kw Rankine cycle aluminum fins, 860° R, 75% fin segments surviving.

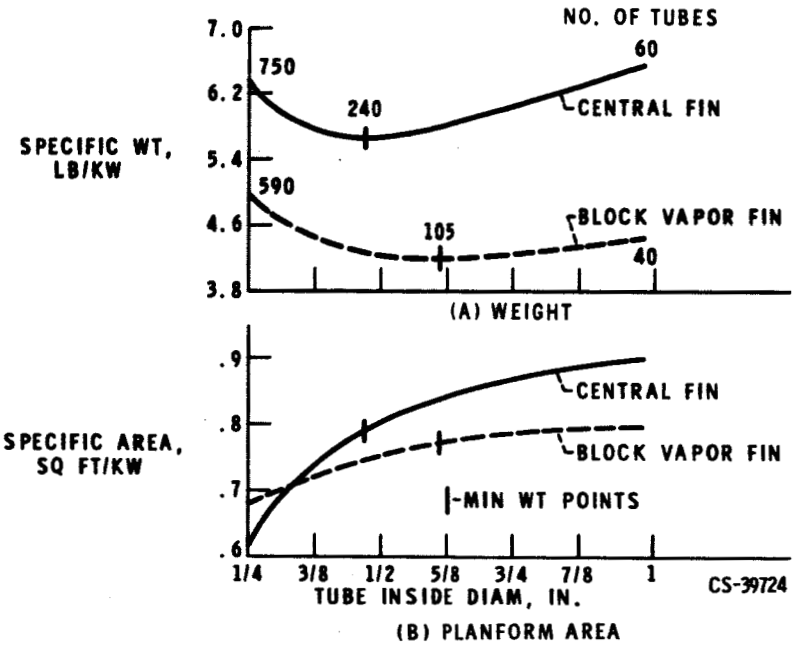

Fig. 10. - Variation of radiator design with tube inside diameter, 500 KW Rankine cycle ss clad copper fins; $P(0)_t$ = 0.98.

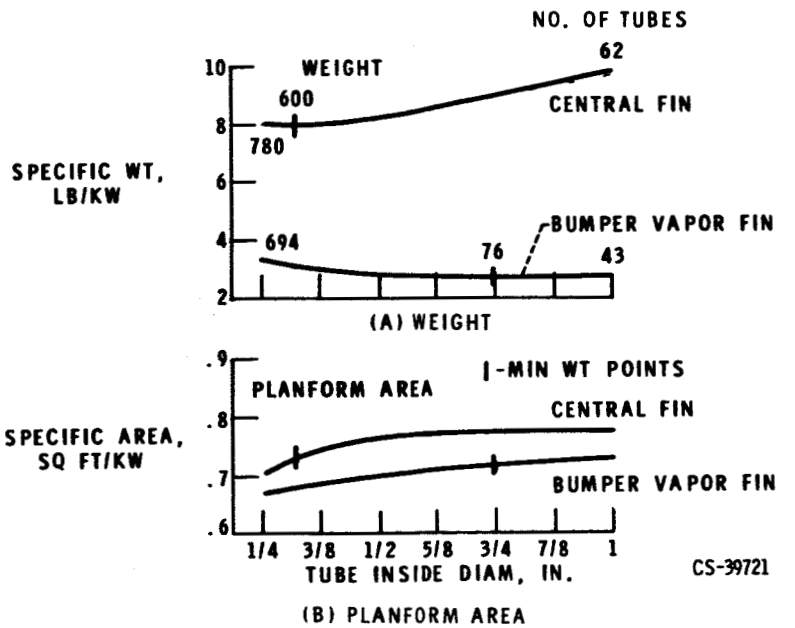

Fig. 11. - Variation of radiator design with tube inside diameter, 500 KW Rankine cycle all stainless steel; $P(0)_t$ = 0.98.

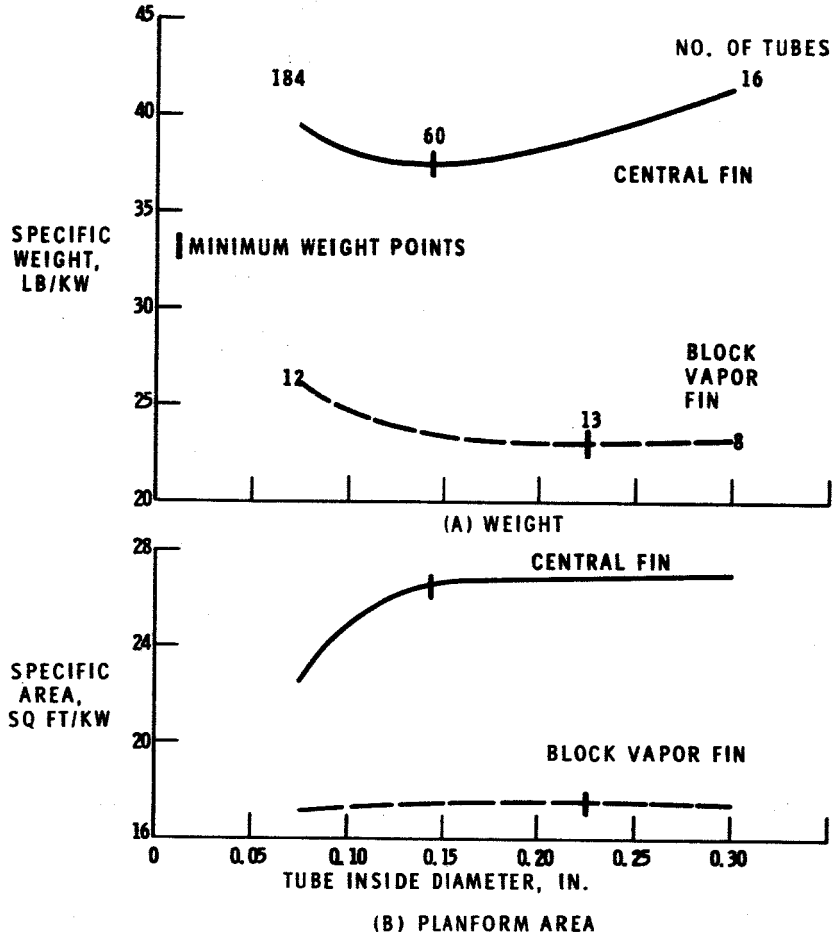

Fig. 12. - Variation of radiator design with tube inside diameter, 30 KW Rankine cycle all aluminum; $P(0)_t = 0.98$.

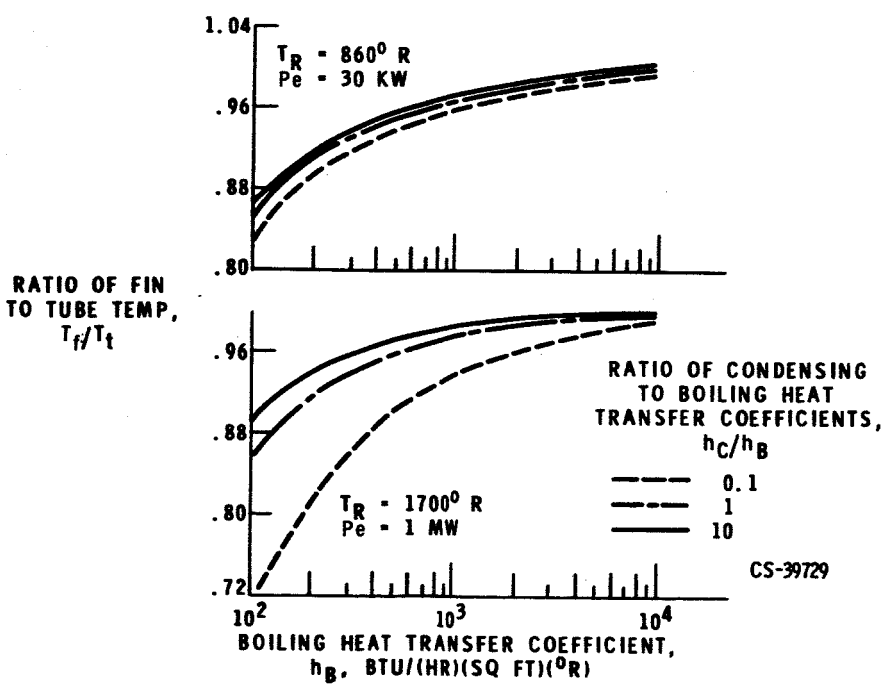

Fig. 13. - Vapor chamber fin temperature.

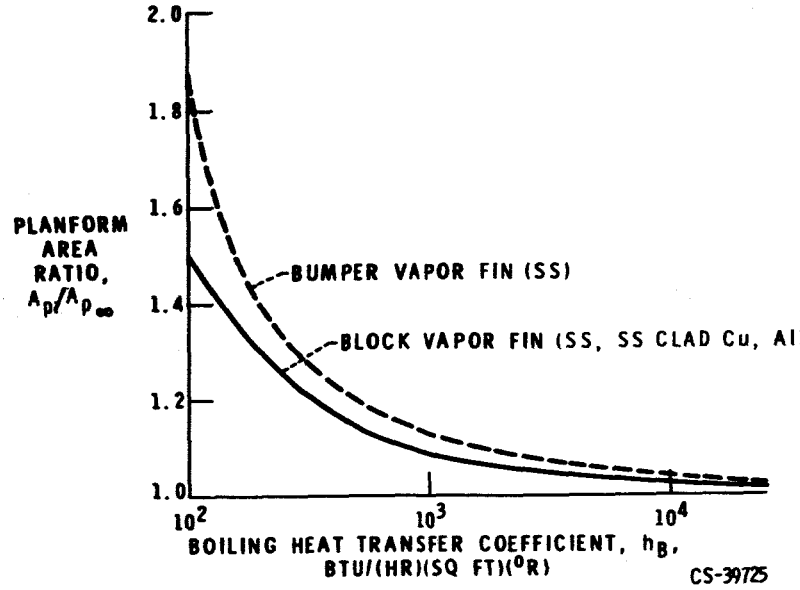

Fig. 14. - Effect of boiling heat transfer coefficient on radiator planform area. $h_C/h_B = 1$.

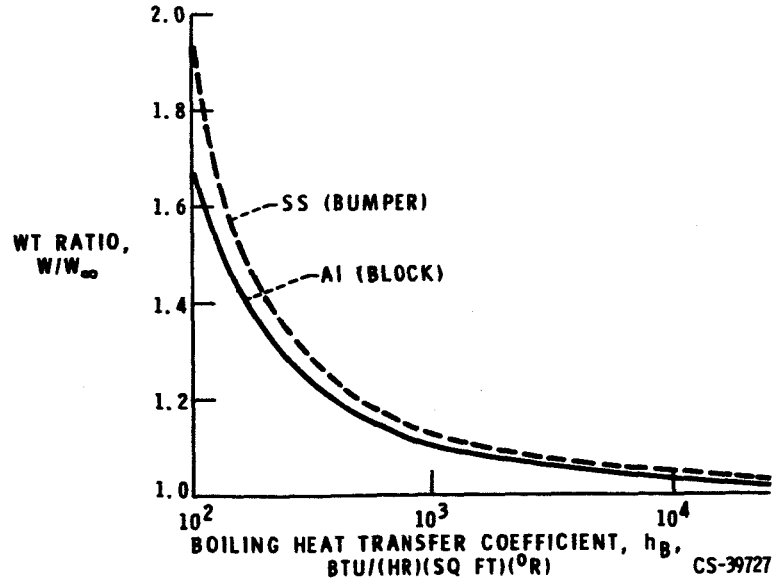

Fig. 15. - Effect of boiling heat transfer coefficient on radiator weight. $h_C/h_B = 1$.

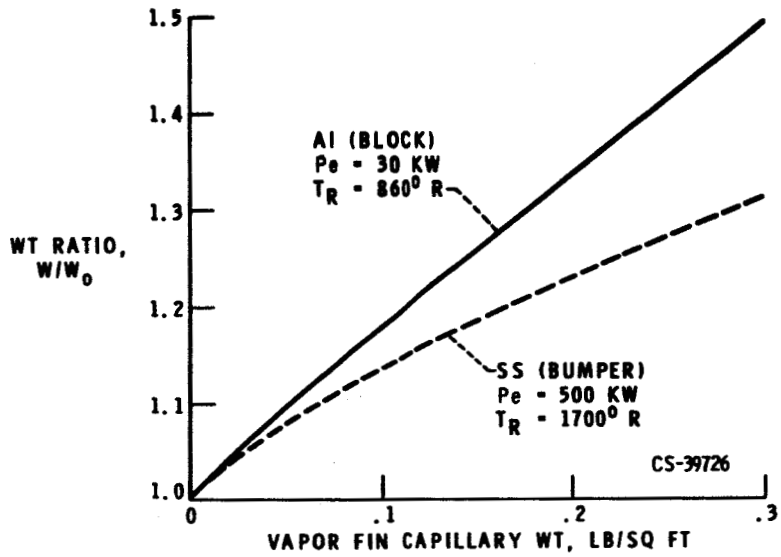

Fig. 16. - Effect of vapor fin capillary weight on radiator weight.